Construction and Building Materials 492 (2025) 142898

Contents lists available at ScienceDirect

Construction and Building Materials

journal homepage: www.elsevier.com/locate/conbuildmat

Understanding the role of calcined clay in yield stress evolution of LC^3 with ultra-high volume of calcined clay and limestone

Yu Chen [a,*], Oğuzhan Çopuroğlu [b,*]

[a] State Key Laboratory of Engineering Materials for Major Infrastructure, School of Material Science and Engineering, Southeast University, Nanjing, China
[b] Microlab, Faculty of Civil Engineering and Geosciences, Delft University of Technology, Delft, the Netherlands

ARTICLE INFO

Keywords:
Structural build-up
Rheology
LC^3
Yield stress
Low-carbon cement

ABSTRACT

Calcined clay plays a critical role in controlling the rheology of limestone-calcined clay cement (LC^3). This study shows that the yield stress of LC^3 mixtures with ultra-high volumes of calcined clay and limestone evolves significantly faster within the first 90 min than that of plain cement pastes at the same solid volume fraction. Two key mechanisms were identified: (1) calcined clay alters particle packing through its layered structure and micro-cavities, promoting physical water absorption; and (2) it enhances interparticle attractive forces via "bridge" formation (C-(A)-S-H bridges and colloidal attractive forces) between cement and calcined clay particles in the fresh state, accelerating rigidification. However, this bridging effect can be hindered by the addition of PCE-based superplasticizers.

1. Introduction

To address growing concerns over CO_2 emissions in the cement and concrete industry, low-carbon cementitious materials have become a focus of research in recent decades [1]. One practical approach is to reduce clinker/Portland cement content using supplementary cementitious materials (SCMs) [2,3]. However, the availability and supply of conventional SCMs, such as fly ash and slag, are becoming a concern for long-term implementation [4,5]. Calcined clay and limestone are considered promising alternatives, offering a low carbon footprint during manufacturing and widespread availability [6]. Concerning the dilution effect on strength and required rheology for mold casting, limestone calcined clay cement (LC^3) typically consists of up to 50 wt% of clinker, along with a blend of calcined clay (30 wt%), limestone (15 wt%) and gypsum (5 wt%) [4,7].

In 3D concrete printing applications, more than 50 wt% of Portland cement/clinker can be replaced by limestone and calcined clay. This is possible because: (1) the size and amount of aggregate are limited by the printing setup and process, resulting in a high content of binding materials in the printable concrete [8,9]. As a result, the strength of the hardened concrete can still be maintained even with more than 50 % clinker replacement; (2) high fluidity of fresh concrete is not a priority. Instead, printable concrete must exhibit sufficient yield stress and rapid structuration after layer deposition (buildability) which is more critical [10]. Our earlier work [8] shows that the buildability of LC3 is significantly enhanced by increasing the calcined clay content (see Fig. 1), attributed to the unique physical characteristics of calcined clay, i.e., its fine grain size, high specific surface area (SSA), and plate-like morphology.

However, it is somewhat arbitrary to attribute the enhancement of the yield stress of LC^3 solely to the physical features of calcined clay. In many earlier studies [8,11–14], Portland cement/clinker is replaced by the mass of calcined clay and limestone, rather than by volume. Due to the lower density of limestone and calcined clay compared to Portland cement, this replacement increases the solid volume fraction (SVF), which also significantly influences the rheology of the fresh mixture. Additionally, beyond SVF, yield stress is dictated by particle interactions, including colloidal attractive forces and C-(A)-S-H nucleation [15,16]. So far, very little attention has been paid to revealing the physicochemical role of calcined clay in the particle interactions of fresh LC^3 mixtures at very early ages. Moreover, the kinetics of these particle interactions in LC^3 has not yet been thoroughly investigated.

This paper aims to explore the role of calcined clay in the static yield stress and structural build-up of fresh cementitious pastes with high-volume of calcined clay and limestone. To achieve this goal, the rheological properties of a ternary blend with varying SVFs (39 %, 43 %, and 55 %), as well as plain Portland cement pastes with an SVF of 43 %, including visco-elasto-plastic behaviors, evolution of static yield stress

* Corresponding authors.
E-mail addresses: y_chen@seu.edu.cn (Y. Chen), O.Copuroglu@tudelft.nl (O. Çopuroğlu).

https://doi.org/10.1016/j.conbuildmat.2025.142898
Received 25 May 2025; Received in revised form 25 July 2025; Accepted 26 July 2025
Available online 30 July 2025

and elasticity with time (first 1.5 h), were quantified and compared. Moreover, the early-age hydration kinetics of studied mixtures were determined by isothermal calorimetry. Finally, plausible mechanisms related to the observed phenomena are discussed in three distinct perspectives, i.e., physical characteristics of particles, particle interactions and rigidification kinetics.

2. Materials and methods

2.1. Raw materials and mix designs

In this study, CEM I 52.5 R Portland cement, limestone powder, calcined clay and gypsum were employed to make the cementitious matrix. Gypsum with more than 99 % purity was supplied by Merck KGaA, Germany. Calcined clay containing high volume of quartz impurity (see Fig. 2(a)) was provided by Argeco, France. As shown in Fig. 2 (b), calcined clay had the coarsest grain size of the fines due to the large particle size of quartz. This was confirmed by the microstructure observation (Fig. 3) and elemental mapping using scanning electron microscopy coupled with energy dispersive spectrometry (SEM-EDS) (Fig. 4). As shown in Fig. 3, three types of calcined clay clusters were observed: (1) quartz particle covered by a layer of agglomerated metakaolin particles; (2) agglomerated metakaolin particles; (3) dispersed metakaolin particles. It should be noted that in this paper, "agglomeration" was mainly used to describe the clusters of undispersed particles. The content of quartz and amorphous phases (mainly metakaolin) was 34.2 wt% and 64.1 wt%, respectively, which was quantified by using quantitative X-ray diffraction analysis using Rietveld refinement method. As mentioned earlier, the presence of quartz impurity in calcined clay can be beneficial to reduce the water demand and to improve the flowability of fresh cementitious materials [17]. Additionally, chemical compositions (as determined by X-ray fluorescence) and physical features of binding materials were summarized in Tables 1 and 2. Calcined clay exhibited extremely high SSA compared to the other fines. Due to the low SSA of quartz impurities, the SSA of the calcined clay used in this study may be relatively low compared to other calcined clays with similar kaolinite content (prior to calcination).

Table 3 presents the mix designs of all studied pastes. For this study, the mixtures can be classified in three groups. The mixtures in the first group had the same solid volume fraction (SVF), including PC, M75, L75, and CC. Mixture M75 contained 25 wt% of Portland cement and 75 wt% of the blend of calcined clay, limestone and gypsum in the binder. The water-to-binder mass ratio (W/B) in mixture M75 was 0.5, which was adjusted in other mixtures to keep the same SVF. The calcined clay-to-limestone ratio was 2.4 for all mixtures except for PC, L75 and CC. The effect of increasing calcined clay and limestone contents on fresh properties was investigated by comparing the test results of mixtures PC and M75. For determining the role of high-volume calcined clay in this context, L75 and CC were considered as reference mixtures. In the second group, mixture M75–1 had a 0.60 of W/B, which largely decreased the SVF from 42.91 vol% to 38.51 vol% compared to mixture M75. The last two mixtures (M75-SP1 and M75-SP2), belonging to the third group, exhibited the same binder compositions and W/B (0.30) but different polycarboxylate ether (PCE)-based superplasticizer (SP) dosages (MasterGlenium®51, BASF). The SP used in this study is in liquid form with a solid concentration of 35 %. This SP was selected to maintain consistency with our previous study [8]. The SVF of both mixtures was about 55 vol%.

As reported by [18,19], sulfate depletion (aluminate peak) may occur before the main hydration peak if there is under-sulfation in LC3 pastes, which may adversely affect the hydration and early-age strength development. Therefore, additional gypsum (4 wt%) was added into mixtures M75, L75, M75-SP1, and M75-SP2 for keeping the similar $CaSO_4$ content to that of mixture PC. The additional gypsum amount was determined by a preliminary isothermal calorimetry screening (see [20]). All fresh paste samples (about 0.5 L each time) used in this study were prepared using the same planetary HOBART mixer and procedures: (1) mix at low speed for 1.5 min after pouring liquid (time zero=the time of adding liquid); (2) pause, scrape the inner wall and bottom of bowl; (3) mix at high speed for 1.5 min.

2.2. Test methods

2.2.1. Isothermal calorimetry test

The hydration heat released in the first 2 days was measured by using a TAM Air isothermal calorimeter. In this test, fresh paste (6 g) was poured into a 20 ml glass vessel after mixing the pre-weighed binder with the water (or water+SP) by a small mixing machine for about 3 min. A reference vessel filled with fine quartz sand (0.125–0.25 mm) together with paste sample vessel were placed in the isothermal calorimeter at 20 °C.

2.2.2. Rheological tests

The rheological tests, including strain sweep, constant shear rate (CSR) and SAOS-time sweep tests, were conducted using an Anton Paar MCR 302e rheometer equipped with a cylindrical cell (inner diameter:

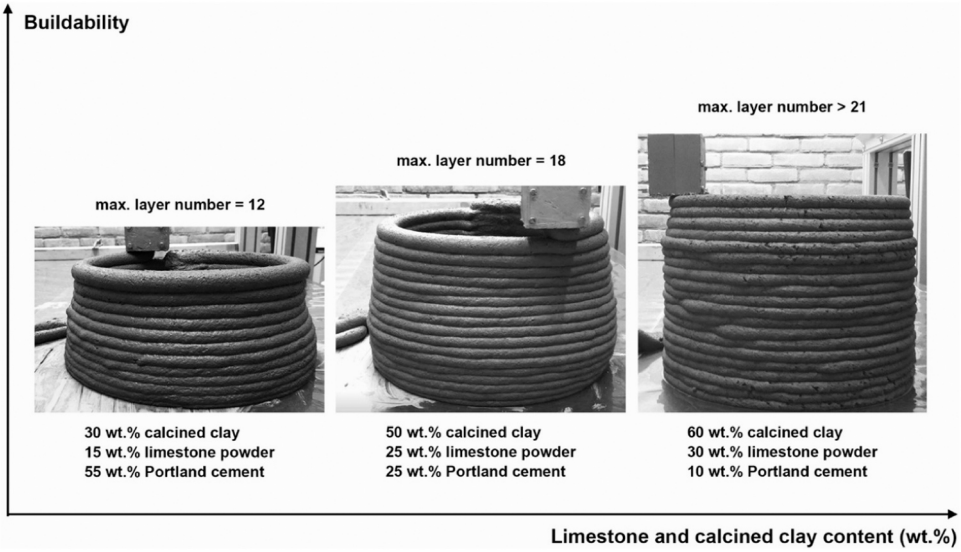

Fig. 1. Buildability performance was enhanced by increasing limestone and calcined clay content (wt%) in printable cementitious materials, adapted from [8].

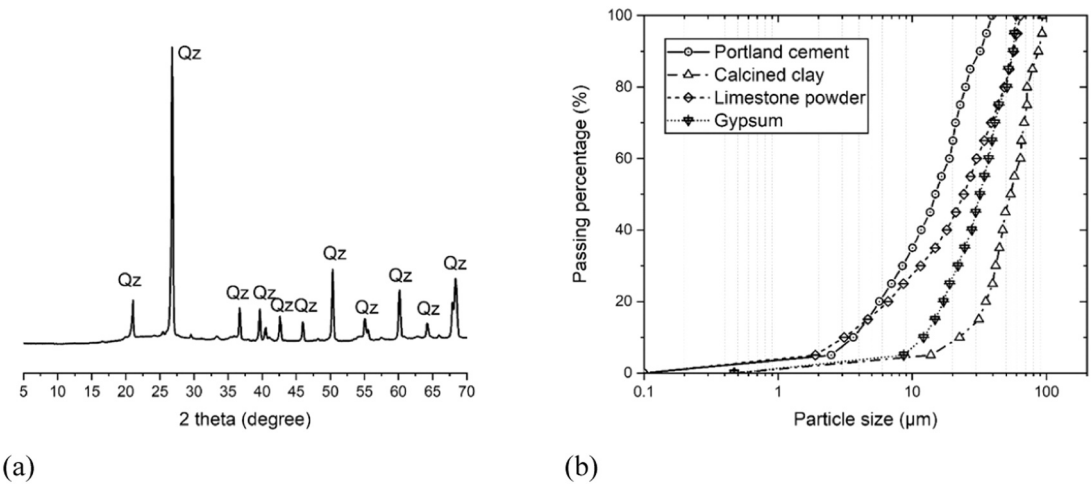

Fig. 2. (a) X-ray diffraction (Cu-Kα radiation) patterns of calcined clay. Qz-quartz. (b) Particle sized distribution of CEM I 52.5 R Portland cement, limestone powder, gypsum and calcined clay measured by laser diffractometry.

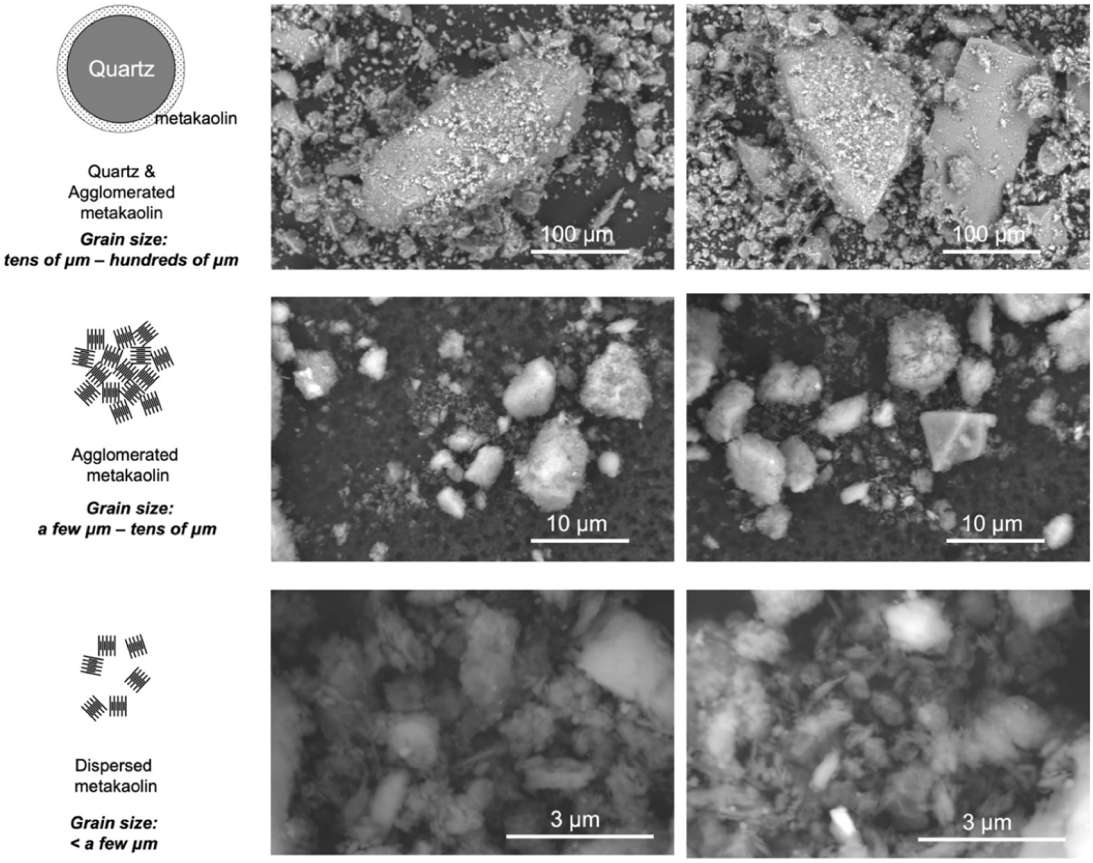

Fig. 3. Particle morphology observation of calcined clay under increasing magnification of secondary electron mode imaging. Three main types of particles were observed: quartz covered by agglomerated metakaolin, agglomerated metakaolin and dispersed metakaolin.

28.92 mm; depth: 68 mm) and a four-blade vane (diameter: 22 mm; height: 40 mm). For each test, about 85 g of fresh paste was poured into the cell. The temperature (20 °C) of the cell was maintained by a Julabo refrigerated circulator. The specific procedures for all rheological tests are summarized and detailed in Table 4.

2.2.2.1. Strain sweep test. After 30 s of pre-shear and resting sessions (material age: 10 min), the applied rotational speed increased linearly from 0 min^{-1} to 100 min^{-1} in 90 s and was kept at the constant rotational speed of 100 min^{-1} for 45 s. Afterwards, the rotational speed was reduced from 100 min^{-1} to 10 min^{-1} in nine consecutive steps (45 s for each step). After waiting for about 10 min, strain sweep test was executed with the applied strain from 0.001 % to 500 % and a frequency of 1 Hz that was also employed by studies [21–23]. The theory of oscillatory shear test can be found in [24,25]. Fig. 5(a) illustrates the typical storage (G') and loss factor (G''/G') vs. applied strain curves. Three regimes can be obtained: liner-viscoelastic domain (LVED), critical strain to flow point, and the domain above flow point (G''>G'). G'

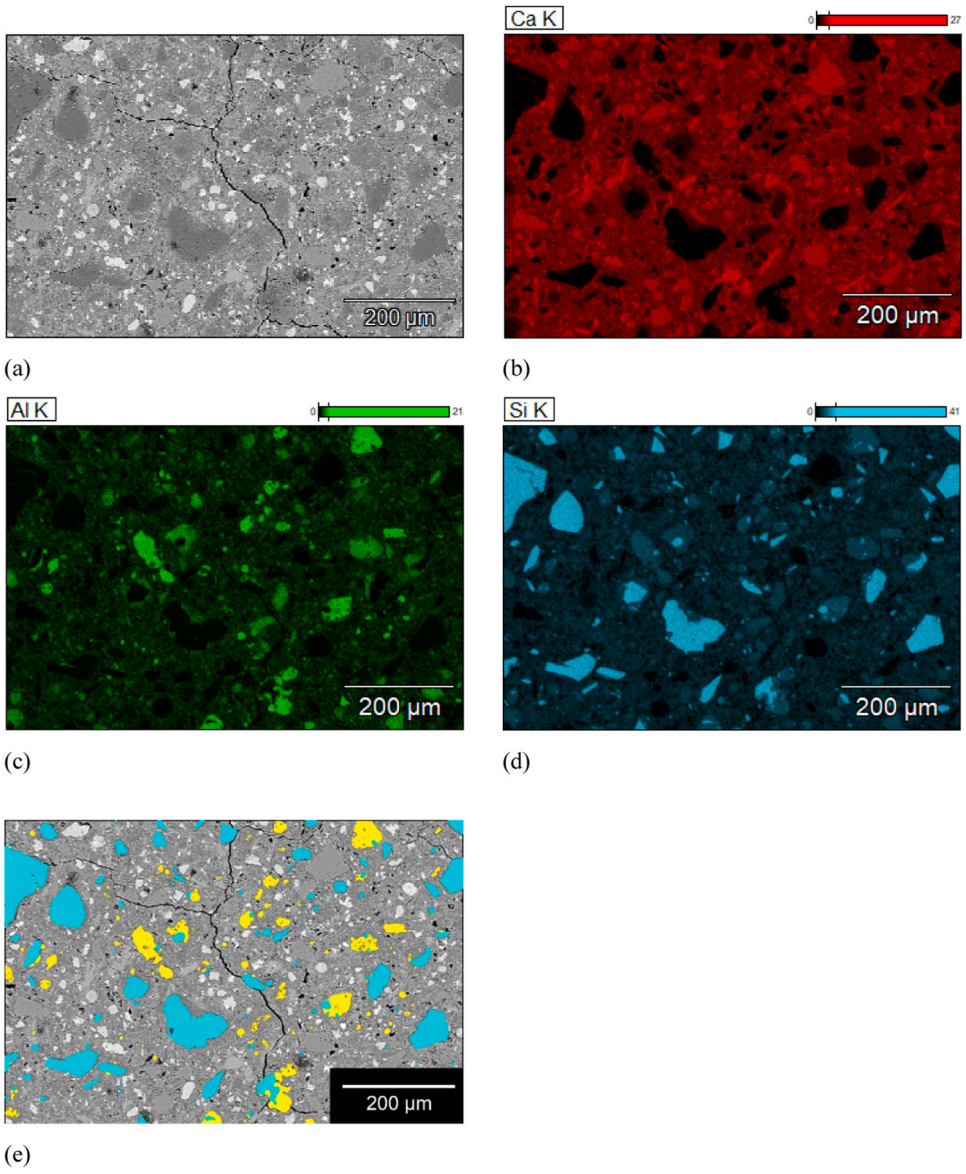

Fig. 4. ESEM-EDS elemental mapping analysis of 28-day LC^3 paste sample (30 wt% calcined clay, 15 wt% limestone, 53 wt% Portland cement, and 2 wt% gypsum, 0.30 of W/B and 0.8 wt% SP): (a) BSE micrograph; (b) Elemental mapping image of Ca (calcium); (c) Elemental mapping image of Al (aluminum); (d) Elemental mapping image of Si (silicon); (e) Overlay masks of quartz (Cyan) and metakaolin (Yellow) particles determined using Compass+XPhase on Pathfinder X-ray Microanalysis Software (Thermo Fisher Scientific).

Table 1
Oxide compositions of calcined clay, limestone powder and Portland cement.

XRF [wt%]	Calcined clay	Limestone powder	Portland cement
CaO	0.54	55.40	67.87
SiO_2	54.38	0.17	17.20
Al_2O_3	37.90	0.03	4.56
Fe_2O_3	2.56	0.04	2.72
K_2O	0.17	0	0.62
TiO_2	1.10	0	0.34
ZrO_2	0.05	0	0
SO_3	0	0	2.41
Others	1.93	0	3.06
L.O.I.	1.37	44.36	1.22

Table 2
Physical characteristics of calcined clay, limestone powder, Portland cement and gypsum.

	Calcined clay	Limestone powder	Portland cement	Gypsum
Density [g/cm^3]	2.51	2.65	3.12	2.32
BET-SSA [m^2/g]	11.19	1.22	1.16	0.53
D_{v50} [μm]	54.09	24.19	14.86	31.94

Table 3
Mixture composition of cementitious materials.

	Portland cement	Calcined clay	Limestone powder	Additional gypsum	Water	SP	Solid volume fraction
	[wt% of the binder]						[vol% of the paste]
PC	100	0	0	0	42.64	0	42.91
M75	25	50	21	4	50	0	42.91
L75	25	0	71	4	48.66	0	42.91
CC	0	100	0	0	52.97	0	42.91
M75–1	25	50	21	4	60	0	38.51
M75-SP1	25	50	21	4	30	0.8	55.18
M75-SP2	25	50	21	4	30	1.2	54.97

SP: superplasticizer.

Table 4
Procedures of rheological tests.

Material age [min:s]	Strain sweep	Material age [min:s]	CSR and Intermittent SAOS	Material age [min:s]	Continuous SAOS
9:00–9:30	Pre-shear 1 (100 min^{-1})	9:00–9:30	Pre-shear (100 min^{-1})	9:00–9:30	Pre-shear (100 min^{-1})
9:30–10:00	Resting	9:30–10:00	Resting	9:30–10:00	Resting
10:00–11:30	Pre-shear 2: Ramp up of rotational speed from 0 to 100 min^{-1}	10:00–10:20	CSR test (0.2 min^{-1})	10:00–90:00	SAOS (0.005 %, 1 Hz)
11:30–19:00	Pre-shear 3: Rotational speed of 100/90/80/70/60/50/40/30/20/10 min^{-1} (40 s for each step)	10:20–10:30	Resting		
19:00–29:40	Resting	10:30–30:00	SAOS (0.005 %, 1 Hz)		
29:40–53:40	Strain sweep test-after 10 min of resting time (0.001 %−500 %, 1 Hz)*	30:00–30:20	CSR test (0.2 min^{-1})		
		30:20–30:30	Resting		
		30:30–50:00	SAOS (0.005 %, 1 Hz)		
		50:00–50:20	CSR test (0.2 min^{-1})		
		50:20–50:30	Resting		
		50:30–70:00	SAOS (0.005 %, 1 Hz)		
		70:00–70:20	CSR test (0.2 min^{-1})		
		70:20–70:30	Resting		
		70:30–90:00	SAOS (0.005 %, 1 Hz)		
		90:00–90:20	CSR test (0.2 min^{-1})		

* The material age for strain sweep test-after 60 min of resting time: 79:40–113:40 [min:s].

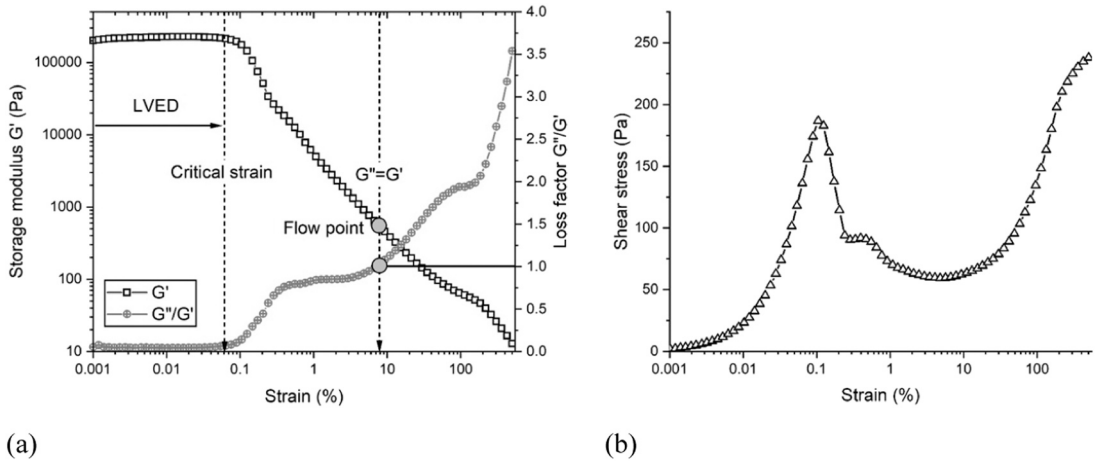

Fig. 5. Strain sweep test: (a) An example curve of storage modulus G' and loss factor G''/G' as a function of applied oscillation strain (0.001 %-500 %); (b) The obtained curve of shear stress and applied oscillation strain (0.001 %-500 %).

showed a relative constant value or small growth in LVED. The critical strain is defined as the end of LVED. According to [15,26], the measured G' is independent of the applied strain within this regime (smaller than the critical strain). Once the applied strain is greater than the critical strain, G' decreases as applied strain increases. The flow point can be obtained when G''=G'. After the flow point (G'<G''), the fresh mixture shows more liquid-like properties [25]. The shear stress (oscillation) vs. applied strain curve was also acquired from this test, as shown in Fig. 5 (b). One or two peaks may appear within about 10 % of applied strain, which seems to be related to the disruption of C-(A)-S-H nucleation and/or colloidal interactions between particles [16,27–29]. The shear stress increased rapidly as the applied strain increased from about 10 % and approached the peak value after 100 % strain is applied. In this regime, the growth and peak of shear stress may be attributed to the hydrodynamic force dominated by the viscosity of liquid phase and/or the direct contact between solid particles induced by inertial effect [28–30].

2.2.2.2. CSR and SAOS tests. CSR-single sample approach was used to quantify the evolution of static yield stress (SYS) within the first of 90 min. About 30 s of pre-shear and resting were also conducted prior to the CSR test. It should be noted that the preshear procedure was applied only prior to the material age of 10 min. At material age of 10, 30, 50, 70 and 90 min, 0.2 min^{-1} of constant rotational speed and 20 s of testing duration were applied. The peak value of each test was defined as the SYS at the specific age. Intermittent SAOS test with 0.005 % strain and 1 Hz (referred to [21]) was performed during the resting time between two consecutive CSR tests for monitoring the elasticity recovery and development of fresh mixtures. In contrast, continuous SAOS with the same testing parameters as the intermittent one was performed on the basis of a new sample from 10 min to 90 min of material age. Fig. 6 shows an example of continuous and intermittent SAOS test results. Owing to the destructive nature of CSR test, the obtained G′ from intermittent SAOS test is smaller than that of the continuous test especially after 30 min. Please also note that the measured SYS using a single sample approach in this work appears to be smaller than that of multi-sample measurements, as discussed by [31,32]. Nevertheless, the applied deformation for each sample at every test cycle was kept identical. CSR-single sample test is still a viable approach to compare the evolution of SYS for different mixtures.

3. Results

3.1. Visco-elasto-plastic behaviors

Fig. 7(a) reports G′ as a function of applied oscillation strain (0.001 %-500 %) for different mixtures after 10 min of resting time. Within LVED, most of mixtures showed a relatively constant G′, whereas mixtures CC, M75-SP1 and M75-SP2 displayed an increase in development with time due to their relatively long percolation times as illustrated in Section 3.2.2. According to Alnahhal et al. [29], the critical strain can be determined by a decrease in G′, which indicated the breakage of network. As shown in Fig. 7(b), the critical strain is in the range of 0.008 %-0.07 % for all studied mixtures. Except for mixture L75, mixtures with the same SVF had the similar critical strain. The critical strain can be increased by increasing SVF, or SP. After the LVED, G′ started to decrease with increasing applied strain. Two humps were determined for most of mixtures (except for mixtures CC, M75-SP1 and M75-SP2) within about 10 % of applied strain. Similarly, they were also observed in the shear stress response at the same applied strain in Fig. 7 (c) (d). The first peak may be attributed to the breakage of rigid network between particles, and the second one can be correlated to the rupture of flocculated particles, according to [16,28,29]. The increase in shear stress after peak 2 seems to be related to the hydrodynamic force and the rigid grain-to-grain contacts between particles. Especially the latter appears to become predominant at large applied strains, contributing to the third peak. Compared to mixture PC, the blended mixture required a higher applied strain to reach both peaks (Fig. 7(c)). Both peak values were summarized in Fig. 7(f). It was found that mixture M75 had the highest peak values compared to the other mixtures. Both peak values slightly decreased by reducing SVF (M75–1) and significantly decreased by replacing calcined clay with limestone (L75).

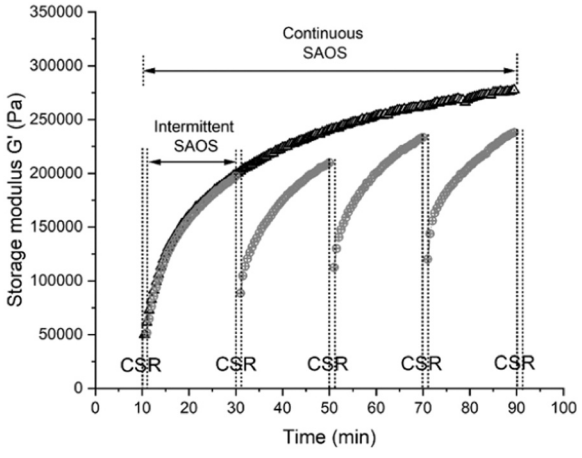

Fig. 6. Comparison between intermittent (CSR test was executed at material age of 10, 30, 50, 70, 90 min) and continuous SAOS tests.

For mixtures CC, M75-SP1 and M75-SP2, only one peak that may be related to the deformation of colloidal interactions can be observed in Fig. 7(c) and (e). For mixtures with SP, the presence of PCEs on the surface of cementitious particles appeared to inhibit C-(A)-S-H nucleation at the very early-age, as reported by [33,34]. The strength of colloidal interaction seemed to be dependent on the competition between attractive colloidal forces and dispersion effect induced by PCEs. The latter was clearly enhanced by increasing the concentration of PCEs. Therefore, mixture M75-SP2 showed a much lower shear stress to break colloidal interactions than mixture M75-SP1.

As shown in Fig. 7(c)–(e), the shear stress showed a decrease trend after the peak related to the breakage of colloidal interactions and then increased rapidly from the applied strain of 10–30 %. The flow point, defined as the crossover point of G' and G'' curves (G′=G''), was determined for most of mixtures in Fig. 7(g). The applied strain at the flow point was reported in Fig. 7(h). For the mixtures with the same SVF, increasing calcined clay content resulted in a higher requirement of applied strain at the flow point, whereas the increase in limestone content significantly reduced that (L75). As discussed in Section 4.1 (Fig. 13), increasing the calcined clay content reduces the water film thickness (WFT), while increasing the limestone content has the opposite effect. A higher WFT facilitates the flow of the fresh mixture, which likely explains the observed trends. The decrease in SVF did not severely affect this strain (mixtures M75 and M75–1). The addition of SP can further increase the required strain to reach the flow point in mixtures M75-SP1 and M75-SP2, whereas the strain was slightly decreased by increasing SP%. In the strain range of 100–500 %, a peak or relatively high value of shear stress was observed in Fig. 7(c) (d) (e), which could be attributed to the hydrodynamic viscous dissipation and/or direct frictional contact between particles [28,30].

3.2. Structural build-up

3.2.1. Evolution of static yield stress

Fig. 8(a) shows the development of SYS of fresh mixtures without SP addition within the first 1.5 h (material age). At 10 min, mixture PC had the highest SYS than others. Mixture M75 displayed a much higher value than that of mixtures CC, L75 and M75–1. A similar SYS was found between mixtures L75 and M75–1, which was lower than mixture CC. After that, the SYS of mixture M75 evolved rapidly and was stronger than mixture PC. Mixture M75–1 had a much higher SYS than mixtures CC and L75. The SYS evolution of mixtures M75-SP1 and M75-SP2 are compared in Fig. 8(b). Mixture M75-SP1 exhibited extremely high SYS at all testing time and had a rapid growth of SYS during the first 50 min. Afterwards, the development of SYS clearly slowed down. A higher SP dosage in mixture M75-SP2 delayed the growth of SYS, resulting in smaller values within the first 1.5 h compared to that of mixture M75-SP1.

3.2.2. Evolution of elasticity and rigidity

Fig. 9(a), (b) report the test results of continuous SAOS, i.e., the evolution of G' and G''/G′ within the first 1.5 h of material age. Similar G' and G''/G′ curve patterns can be found in mixtures without SP addition (except for mixture CC). Two regimes were determined: (1) G' and G''/G′ evolved rapidly within the first 10 min of resting time; (2) Afterwards, the growth of G' became slower, and G''/G′ approached zero. The first regime seems to be related to the formation of a network induced by the flocculation of cementitious particles at rest, and the

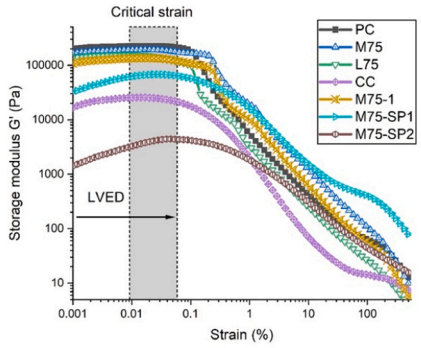

(a)

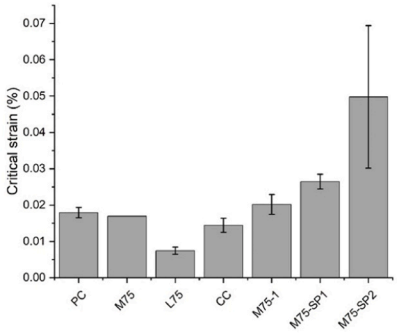

(b)

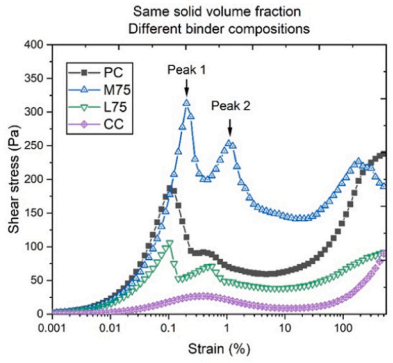

(c)

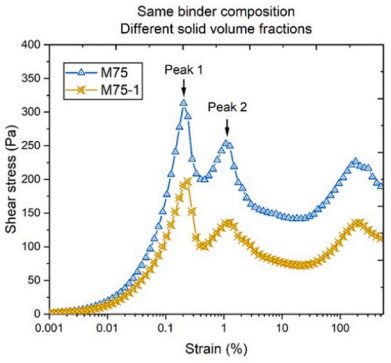

(d)

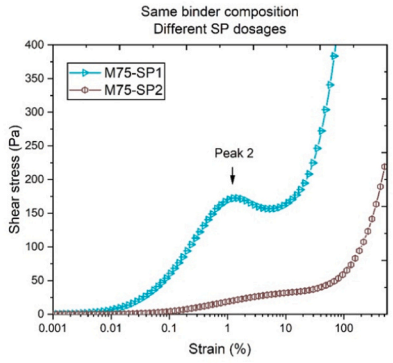

(e)

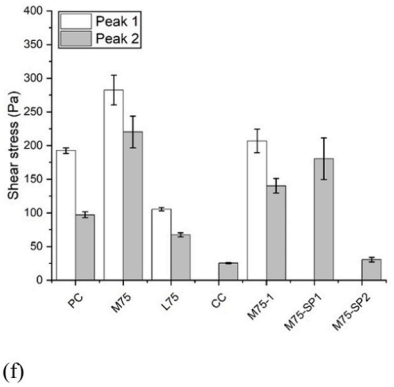

(f)

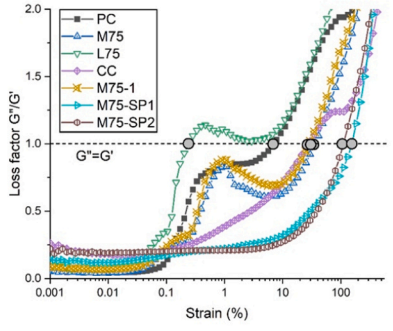

(g)

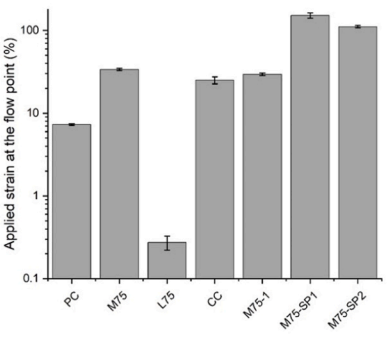

(h)

(caption on next page)

Fig. 7. Strain sweep test results: (a) G′ vs. applied oscillation strain (0.001 %-500 %); (b) Critical strain (end of linear-viscoelastic domain) of different mixtures; (c) The obtained shear stress under applied oscillation strain (0.001 %-500 %)-mixtures with the same solid volume fraction but different binder compositions; (d) Mixtures with the same binder compositions but different solid volume fractions; (e) Effect of different dosages of SP; (f) A summary of the required shear stress to reach peak 1 and peak 2. (g) Loss factor vs. applied strain (0.001 %-500 %); (h) Applied strain at the flow point (G′=G′′). Error bars represent the standard deviation of repeated test results.

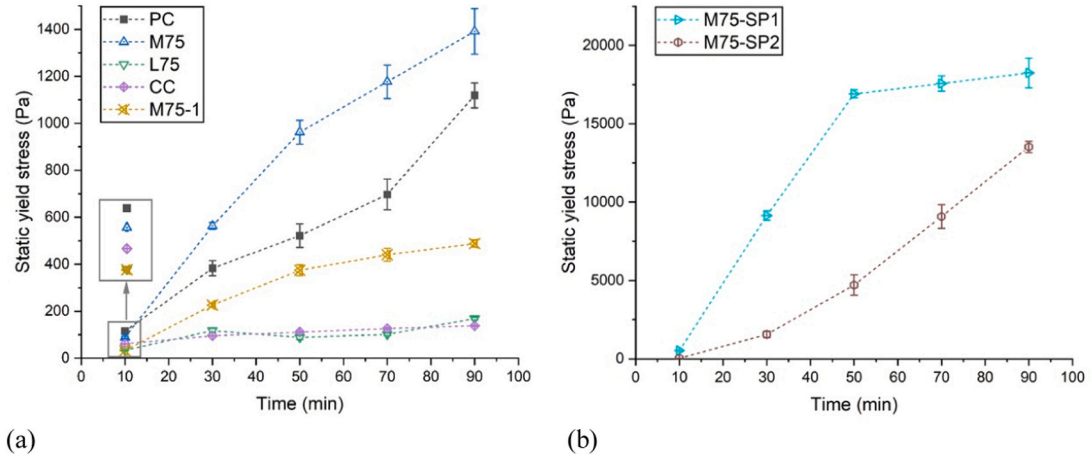

Fig. 8. CSR test results: (a) Static yield stress development within the first 1.5 h of mixtures without SP addition; (b) Static yield stress development within the first 1.5 h of mixtures containing SP. Error bars represent the standard deviation of repeated test results.

second one can be attributed to forming a rigid percolated network, as explained by Roussel et al. [16]. G' of mixture M75 developed slower compared to mixture PC which seems to contradicting with the SYS results. According to earlier studies [26,35], a high G′ is not necessarily coincident with a high SYS due to different testing mechanisms. The strain sweep test results (Fig. 7(a), (c)) show that mixture M75 also exhibited a lower G′ within the LVED regime but a higher shear stress (peaks 1 and 2) than mixture PC. Additionally, the G′ in SAOS depends only on the elastic response of 0.005 % amplitude strain, which is dominated by the energy transferring capacity of a rigid percolated network. This capacity appears to be related to the formation of C-(A)-S-H bridges and other precipitates (e.g., ettringite and hydrated aluminates). Clearly, mixture PC, with its high concentration of chemical species, is expected to show a fast G′ evolution. In contrast, the SYS is defined as the required shear stress to reach flow onset, which requires a much larger applied strain than that in SAOS. Energy dissipation caused by disrupting particle interaction (C-(A)-S-H bridges and colloidal attractive forces) and friction for initiating relative motion between particles plays a critical role in this context. Therefore, as shown in Fig. 10, the increase of G′ in SAOS arises from the increasing number of "bridges" in the cementitious particle system, whereas the SYS depends on not only the number of "bridges" but also the strength of these "bridges" (particle interactions) and even rigid grain-to-grain contacts. Further discussion was provided in Section 4.2. Replacing calcined clay by limestone (L75), or decreasing SVF (M75–1) negatively affected the growth of G′ with time, in comparison with mixture M75. The inter-particle distance was increased for both mixtures (see Section 4.1) and the concentration of chemical species (sourced from Portland cement) was diluted in mixture M75–1. For mixture CC, the development of G′ and G′′/G′ can be linked to the particle percolation induced by sedimentation.

In contrast, mixtures containing SP showed different G′ and G′′/G′ curve patterns (three regimes). Both mixtures experienced a regime of slow growth in G' and G′′/G′, prior to the rapid development. This regime appears to be caused by the retarding effect of SP, i.e., steric hindrance, on flocculation [33,34,36], which was extended by the increase in SP dosage. In addition, the slope of G′ development in the fast evolution regime was also reduced by the presence of SP. However, mixture M75-SP1 reached the similar elasticity (G') and rigidity (G′′/G′) at 1.5 h compared to mixture PC, due to the relatively high SVF. To indicate the transition between two regimes, percolation time was defined according to [37,38] and computed using the derivative value of loss factor as shown in Fig. 9(c). Fig. 9(d) summarizes the percolation time of different studied mixtures. Similar percolation times were found for mixtures PC and M75. The percolation time can be extended by lowering the SVF (M75–1), increasing limestone content (L75), or adding SP. The addition of SP played a more dominant role on increasing percolation time than other factors.

Fig. A1 (a)-(h) compare the G′ development with time using continuous and intermittent SAOS approaches. Clearly, CSR measurement can disturb the elasticity and rigidity evolution of fresh cementitious pastes, resulting in a much smaller G′ after each test cycle (after 30 min) compared to the value obtained by the continuous method, which agreed well with the earlier studies [23,27]. The last value of each G′ evolution curve (before each CSR test cycle) from intermittent SAOS test was compared with that of continuous SAOS test in Fig. 11. As can be observed, the mixture with a fast G′ growth in the continuous SAOS test (see Fig. 11 (a)) also displayed large values in the intermittent SAOS test. This can confirm that test results obtained from CSR-single sample measurement and intermittent SAOS are still feasible to compare structural build-up of various mixtures. Fig. 11 (b) presents the difference in G′ between continuous and intermittent SAOS tests at the different material ages. For different mixtures, the influence of CSR testing on the G′ is not the same. Except for mixture CC, the mixture with a relatively high Portland cement content showed a fast G′ recovery. This implies a relatively small interference on the structuration of fresh mixture. The presence of SP causes a significant delay of G′ recovery resulting in a huge difference between G'_c and G'_i. For mixture M75-SP1, this effect becomes minor at 90 min compared to earlier ages.

3.3. Early-age hydration kinetics

Fig. 12(a) reports the normalized heat flow of studied mixtures over the first 2 days. Mixtures PC and M75–1 showed a similar duration before the main hydration peak. In contrast, for mixtures M75, M75–1 and L75, the main hydration peak appeared about two hours earlier, which may be considered as the filler effect of calcined clay and/or limestone, as reported by [14,39]. Increasing the content of limestone

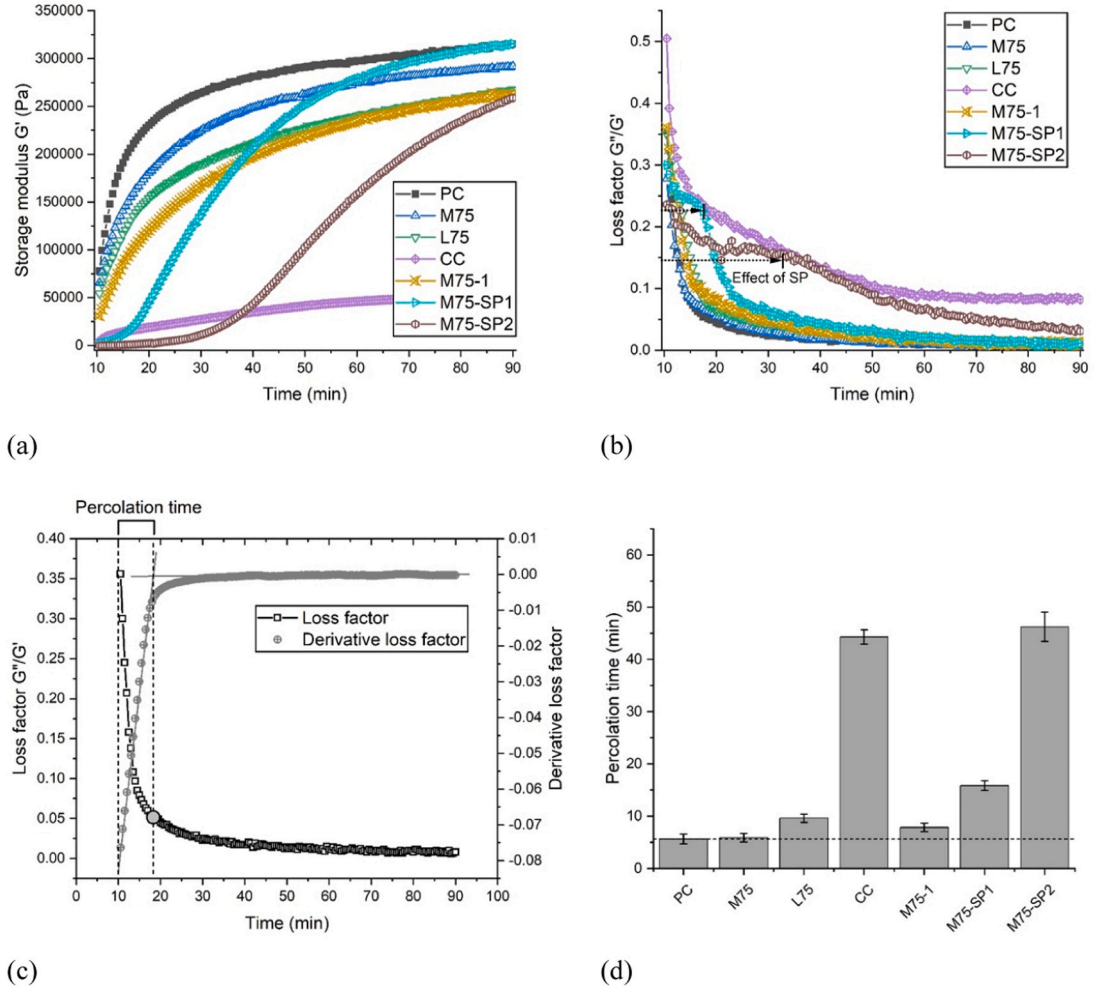

Fig. 9. Continuous SAOS test results: (a) G' evolution with time of different mixtures; (b) G''/G' evolution with time of different mixtures; (c) The derivative value of loss factor was employed to determine the percolation time; (d) Percolation time of different mixtures. Error bars represent the standard deviation of repeated test results.

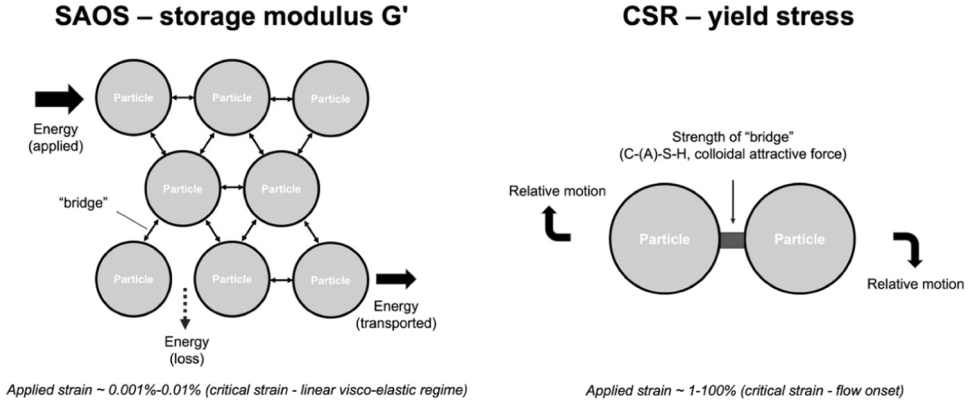

Fig. 10. (Left) Illustration of testing mechanism of SAOS. The magnitude of G' appears to be dominated by the number of "bridge"; (Right) Illustration of testing mechanism of CSR. The static yield stress is related to the strength of particle interaction ("bridge") and in some cases, is also influenced by the solid contacts between particles during the relative motion.

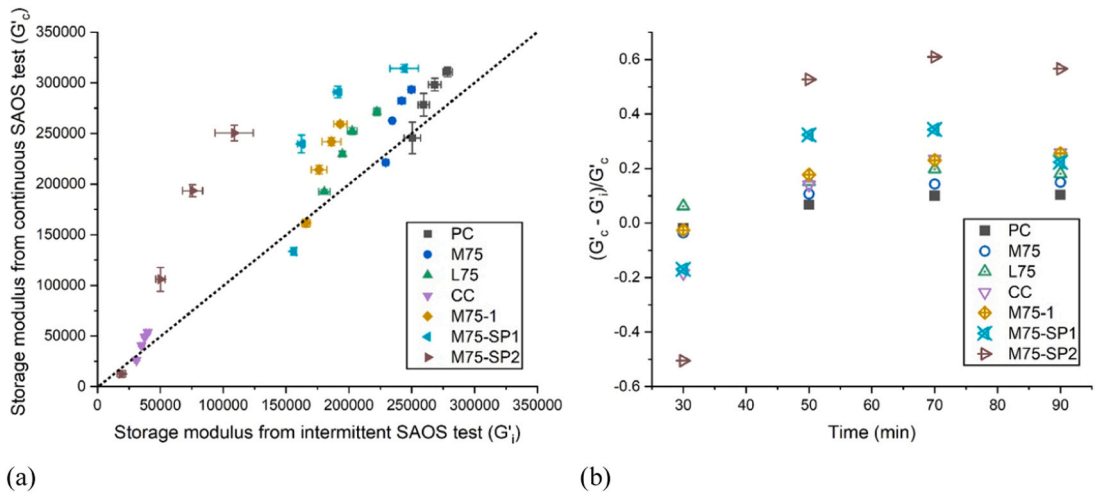

Fig. 11. (a) Correlation between storage moduli from intermittent SAOS test (G'_i) and continuous SAOS test (G'_c). The dashed line indicates that both values are equal; (b) The reduction of G' caused by CSR test ((G'_c - G'_i)/G'_c) after each cycle. Error bars represent the standard deviation of repeated test results.

and calcined clay also decreased the intensity of the peak caused by the dilution effect. The addition of SP delayed the time of the main hydration peak but did not modify the intensity. For mixtures containing calcined clay, a small peak or shoulder was observed at 28 h (except for mixtures M75–1 and M75–2, the time was delayed about 3–7 h), which can be attributed to the aluminate peak due to the temporary sulfate depletion [40]. As shown in Fig. 12 (b), the cumulative heat of hydration was increased by the increase in PC content. Compared to mixture L75, mixtures with 50 % of calcined clay (M75, M75–1, M75-SP1 and M75-SP2) showed much higher cumulative heat value from 24 h of hydration. Such an increase can be caused by the aluminate-sulfate and pozzolanic reactions induced by the calcined clay.

To study their very early-age hydration, the normalized heat flow over the first 4 h was illustrated in Fig. 12 (c). Within the first 1 h, the intensity of normalized heat flow decreased rapidly with time. The decrease in Portland cement content reduced the normalized heat flow value. Compared to mixture L75, mixtures with calcined clay showed a higher intensity of normalized heat flow. The required time to the onset of acceleration stage for different mixtures was summarized in Fig. 12 (d). It can be found that mixtures PC and L75 required the similar resting time. In contrast, the addition of calcined clay clearly extended the dormant period. Such a delay may be related to the aluminate ions released from metakaolin dissolution which can inhibit C_3S dissolution, as reported by [41]. Besides, calcium hydroxide (CH) can also react with metakaolin to form C-A-S-H gel, resulting in the decrease of Ca^{2+} concentration in the pore solution [4]. Adding SP further delayed the onset of acceleration stage. The increase in normalized cumulative heat (10–90 min) of different mixtures was summarized in Fig. 12 (e). The relationship between the increase in cumulative heat and the increase in G' (Continuous SAOS-time sweep test results) was indicated in Fig. 12 (f). For the mixtures without SP, a near linear correlation can be found between these two values. As mentioned earlier, adding SP significantly reduced the initial G' and delayed the hydration. However, the G' in mixtures M75-SP1 and M75-SP2 evolved rapidly, which may be related to the small particle distance caused by the high SVF.

4. Discussion

4.1. Effect of physical characteristics of particles on static yield stress

The SYS of fresh mixtures at a very early age appears to be primarily governed by colloidal attractive forces, the formation of C-(A)-S-H bridges, and solid particle contacts [35,42]. The physical features of binder particles, i.e., particle size, SSA, and packing density, can severely influence one or all of factors as mentioned above. Water film thickness (WFT) as one indicator can be used to describe most of physical characteristics of binder particles at the original stage (without considering hydration), as proposed by [43,44]. According to studies [14,45], WFT also indicates the inter-particle distance, which severely influences SYS of fresh mixture. The low WFT is usually correlated to a low flowability and high SYS (see Refs [14,46,47]).

$$SSA_{total} = SSA_P R_P + SSA_C R_C + SSA_L R_L + SSA_G R_G \quad (2)$$

$$WFT = \frac{W_0 - W_m}{SSA_{total}} = \frac{\frac{1-\phi}{\phi} - \frac{1-\phi_{max}}{\phi_{max}}}{SSA_{total}} = \frac{\frac{1}{\phi} - \frac{1}{\phi_{max}}}{SSA_{total}} \quad (3)$$

where SSA_P, SSA_C, SSA_L, and SSA_G represent the specific surface area (m^2/g) of Portland cement, calcined clay, limestone powder, and gypsum. R_P, R_C, R_L and R_G are their volume proportions to the total solid volume. W_0 and W_m mean the water ratio of the paste (water volume/solid volume) and the void ratio (void volume/solid volume), respectively. ϕ and ϕ_{max} denote the SVF and the maximum SVF of studied mixtures. Fig. 13 (a) shows the SSA_{total} of studied mixtures. As can be observed, the mixture with the same binder composition has the similar value (M75, M75–1, M75-SP1 and M75-SP2). Owing to the very high SSA of calcined clay, mixture CC displayed the highest SSA_{total} compared to others and mixture M75 showed a much higher value than mixture PC. The addition of limestone powder resulted in a decrease in SSA_{total} (L75). As mentioned by Ref [48], ϕ_{max} is difficult to be quantified using an experimental approach. In this study, the value of ϕ_{max} is assumed in the range of 0.55–0.7 for all studied mixtures (this range was made according to [28,30]). The computed WFT was summarized in Fig. 13 (b). Mixtures M75, M75–1, M75-SP1 and M75-SP2 with the same binder composition should have the similar ϕ_{max}. Thus, their WFTs are solely depended on the SVF. A high SVF led to a low WFT. One may debate that the presence of SP may increase ϕ_{max}. As shown in Fig. 13 (b), when ϕ_{max} of M75-SP1 or M75-SP2 is 0.7 and ϕ_{max} of M75 is 0.55, WFT of M75-SP1 or M75-SP2 is still lower than M75. Thus, the effect of SP on ϕ_{max} is considered negligible in this context. Mixtures PC and L75 exhibited a much higher WFT than mixtures with calcined clay. By comparing the SYS and WFT of different mixtures, it can be seen that a low WFT does not always correspond to a high SYS in this study, especially for mixtures M75 and PC at 10 min. It must note that WFT of mixtures may be underrated since the agglomeration of particles was not considered in the calculation.

As mentioned in Section 2.1, calcined clay used in this study is a blend of coarse quartz and fine metakaolin. The quartz particle with a coarser grain size than limestone could increase pore size between

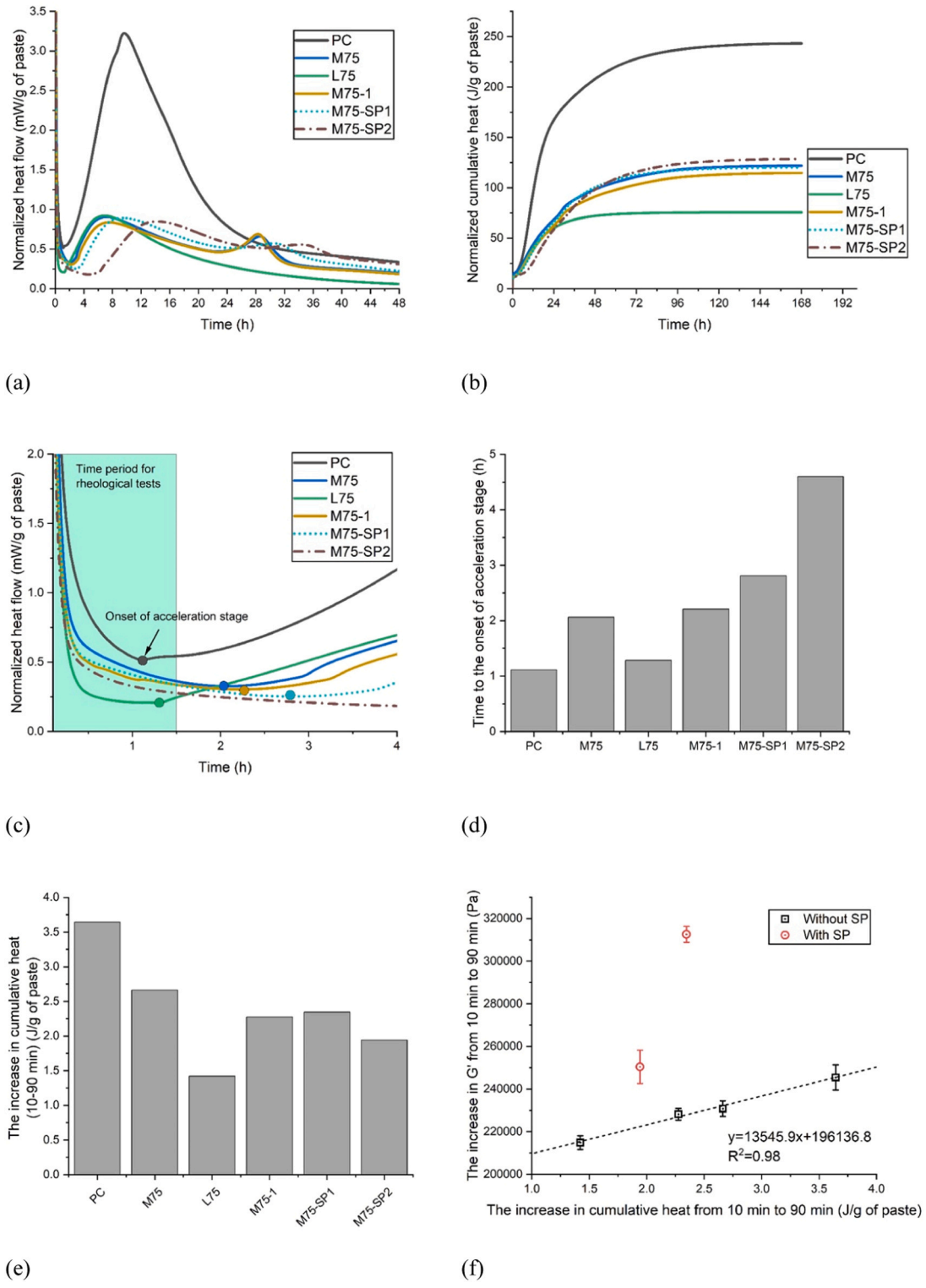

Fig. 12. Isothermal calorimetry test results: (a) Heat flow normalized by paste weight over 2 days; (b) Cumulative heat normalized by paste weight over 7 days; (c) Heat flow normalized by paste weight over the first 4 h; (d) The summary of the required time to the onset of acceleration stage; (e) The increase in cumulative heat from 10 min to 90 min; (f) The correlation between the increase in cumulative heat and the increase in G′ (Continuous SAOS-time sweep test results) from 10 min to 90 min.

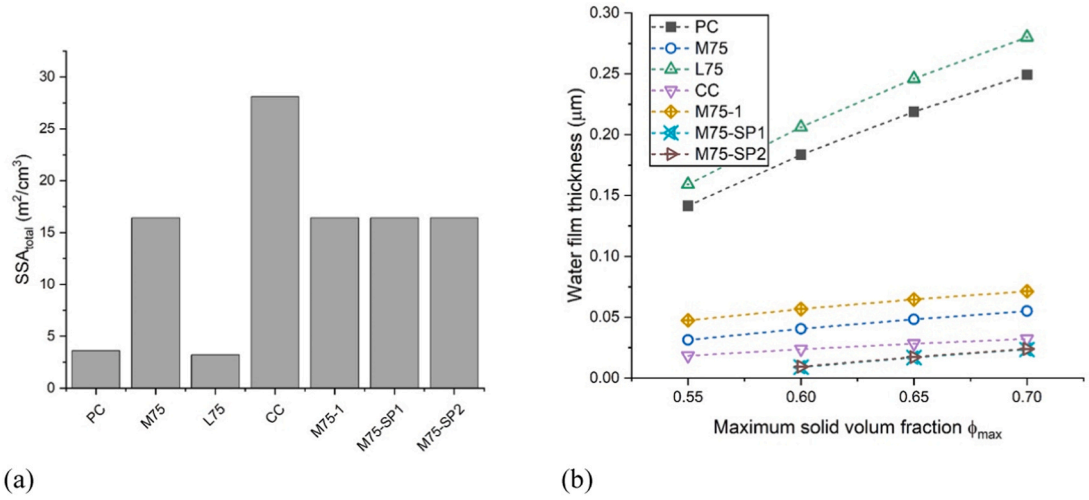

Fig. 13. (a) The total specific surface area (SSA_{total}) of different mixtures; (b) The water film thickness (*WFT*) of different mixtures by assuming the maximum solid volume fraction (ϕ_{max}) in the range of 0.55–0.7.

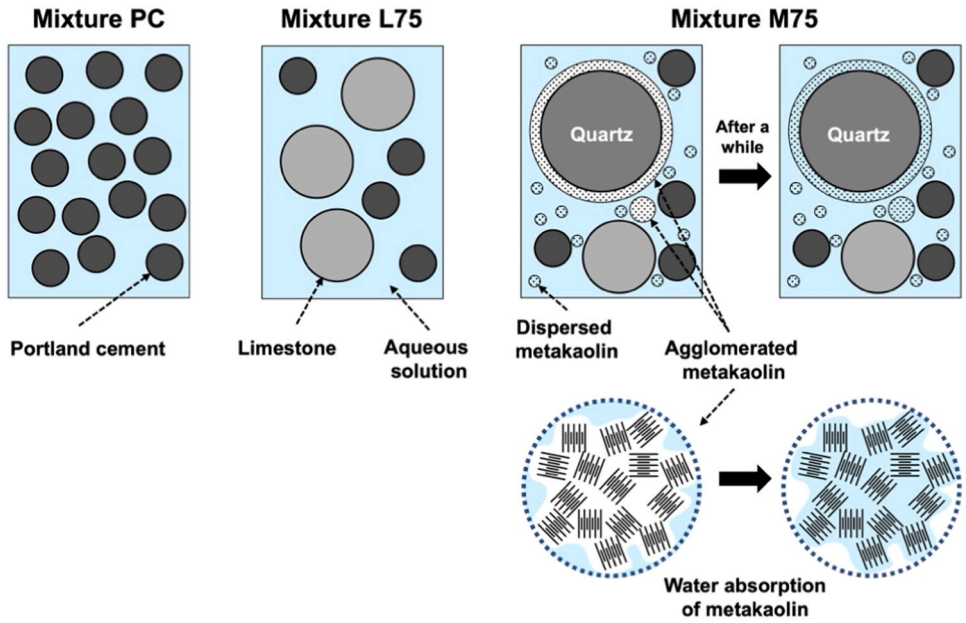

Fig. 14. Illustration of particle systems of mixtures PC, L75 and M75. For mixture M75, the cluster of agglomerated metakaolin particles with a card-house structure could absorb free water over time.

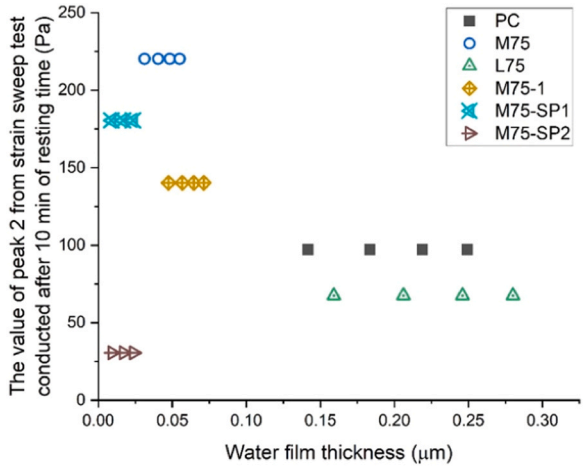

Fig. 15. The relationship between water film thicknesses and the value of peak 2 from strain sweep test-after 10 min of resting time.

particles. By contrast, due to its fine grain size, metakaolin is expected to reduce pore size, thus counteracting the effect of coarse quartz on pore size. However, the fine particles of metakaolin are prone to agglomeration, which can cause them to adhere to quartz surfaces or cluster together. When this happens, the surface area of the metakaolin is greatly reduced, and initially, a card-house structure is formed that contains many unfilled micro-cavities. This can temporarily increase the free water content and result in a lower SYS (a higher WFT than the expected value) compared to the PC mixture at the beginning. Over time, these agglomerated clusters of metakaolin absorb free water (see Fig. 14). Additionally, the absorbed water in the agglomerated metakaolin particles seems to be stored properly and cannot contribute to the fluidity of the mixture, which could be one of the reasons for the higher SYS of mixture M75 from 30 min when compared to mixtures L75 and PC.

4.2. *Effect of particle interactions on static yield stress*

According to [16,49,50], the non-retarded van der Waals interaction

is considered to dominate other colloidal interactions for cementitious pastes and the attractive energy potential Φ_0 can be given as:

$$\Phi_0 \cong \frac{A_0 a^*}{12H} \quad (4)$$

where A_0 denotes the non-retarded Hamaker constant; a^* means the radius of curvature of the "contact" points and H represents the surface-to-surface separation distance. For a cementitious material system, A_0 and a^* are fixed values and therefore, the van der Waals attractive interaction mainly depends on H. In the case where all particles are suspended in aqueous solution, WFT is considered as the similar term of H. As mentioned in Section 3.1, one or two peaks of shear stress appeared within a few percent of applied oscillation strain (Fig. 7(c)-(e)). Peak 1 is only found in the mixtures containing Portland cement without SP and peak 2 exists in all mixtures. According to [16,28,29], peak 1 is probably correlated to the rigid interaction caused by C-(A)-S-H nucleation. PCEs covering the surface of Portland cement delayed the formation of C-(A)-S-H bridges [34], resulting in the absence of peak 1 in mixtures with SP. Peak 2 appears to be dictated by colloidal interactions. The relationship between WFT and Peak 2 is shown in Fig. 15. For mixtures without SP (except for CC), an increase in WFT resulted in a reduction of shear stress induced by colloidal interactions (Peak 2). The presence of SP in mixtures M75-SP1 and M75-SP2 enhanced the dispersion force caused by steric hindrance, which weakened the colloidal attractive force. The decrease in Peak 2 seems to be amplified by increasing the SP dosage.

However, mixture M75-SP1 displayed the highest SYS compared to others within the first 90 min. This may be attributed to the high solid contact forces between particles during CSR testing. As shown in Fig. 16, to reach the critical strain of flow onset (peak value of CSR curve), mixtures with SP require a much higher applied strain than that of mixtures without SP. Please note that the applied (oscillation) strain cannot be regarded as the "real" deformation of tested material due to the existence of strain lag [32,51]. For mixtures M75-SP1 and M75-SP2, the applied strain at the flow onset in CSR test is much larger than the

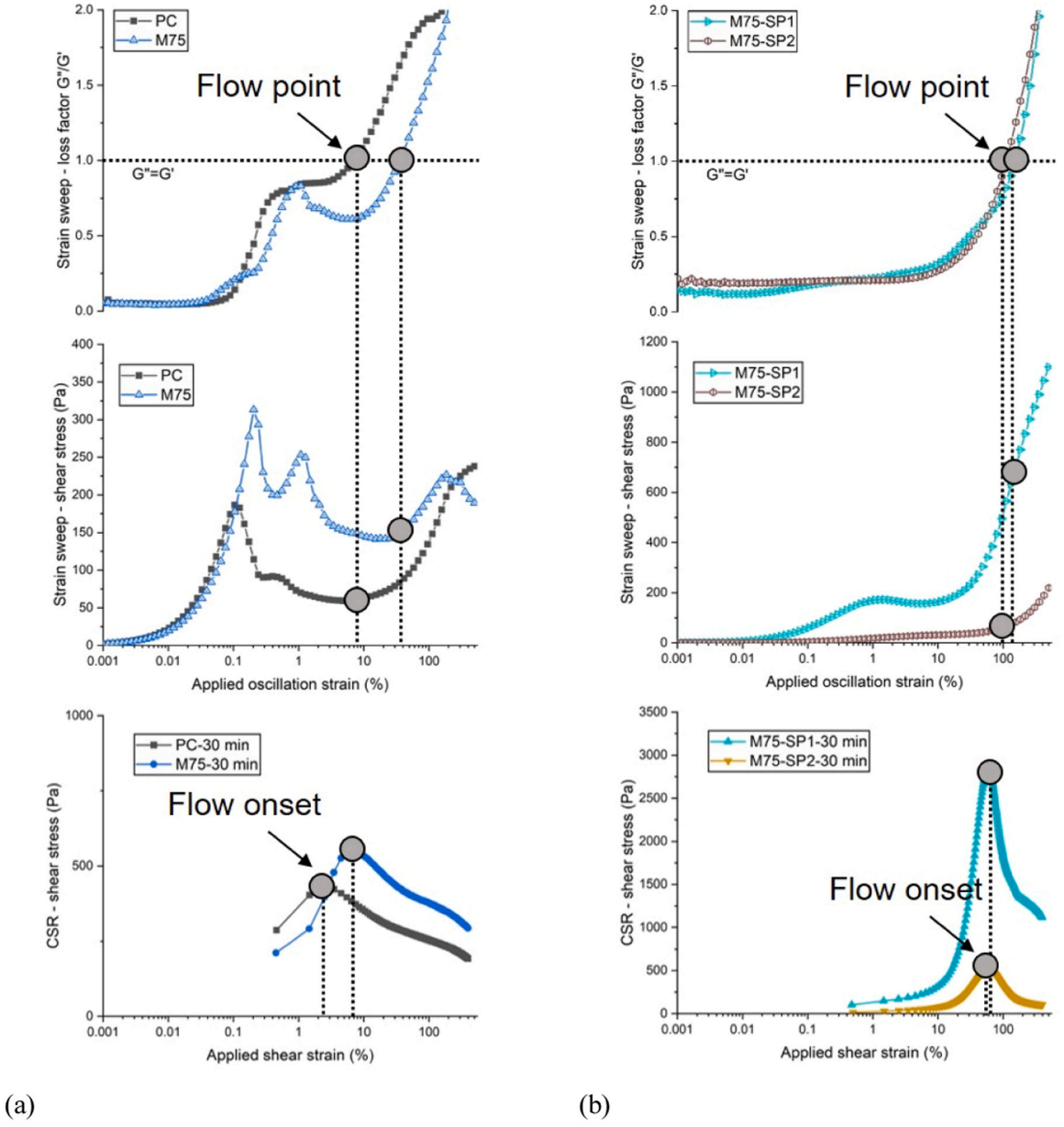

Fig. 16. The applied oscillation strain at the flow point from strain sweep test (conducted at material age of about 30 min) and applied shear strain at the flow onset from CSR test (conducted at material age of 30 min): (a) Mixtures without SP (PC and M75); (b) Mixtures with SP (M75-SP1 and M75-SP2).

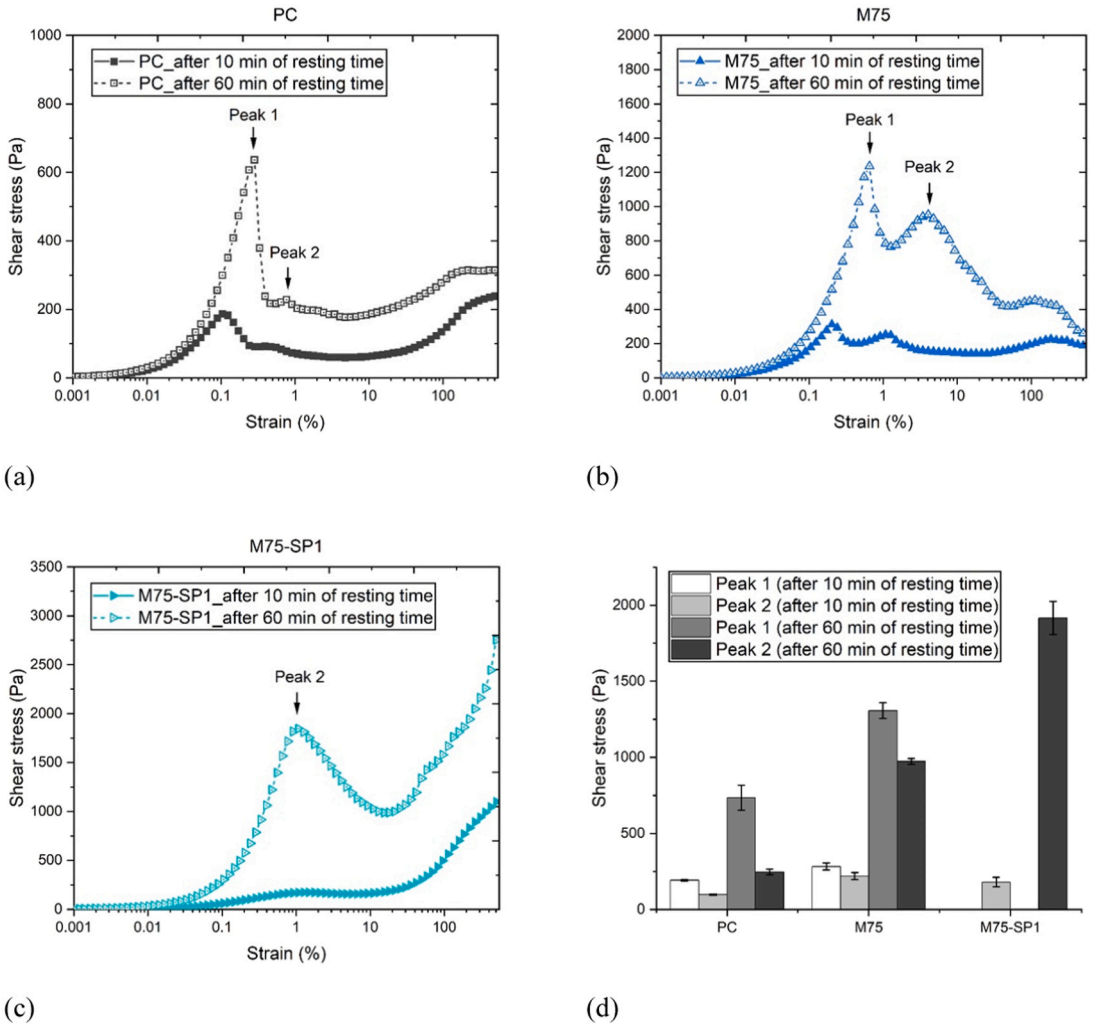

Fig. 17. Strain sweep test results of mixtures PC, M75 and M75-SP1 performed after 10 min (material age: 29–53 min) and 60 min (material age: 79–113 min) of resting periods. The obtained shear stress under applied oscillation strain (0.001 %-500 %): (a) mixture PC, (b) mixture M75, and (c) mixtures M75-SP1; (d) A summary of peak 1 and peak 2. Error bars represent the standard deviation of repeated test results.

strain of peak 2 and smaller than that of flow point in strain sweep test. The shear stress increased with applied strain immediately after peak 2. Compared to the value of peak 2, a comparable or even larger shear stress caused by rigid grain-to-grain contacts is found in the range of 10–100 % of applied oscillation strain. Thus, the solid contacts are hypothesized to play a significant role in SYS of mixtures M75-SP1 and M75-SP2, owing to their small particle distances (high SVF). In the case of mixtures without SP (PC and M75), the applied shear strain at flow onset is also greater than the strain at peak 2 but less than the strain at the flow point. However, the shear stresses at peaks 1 and 2 are much higher than that at the applied strain at the flow point. Clearly, the measured SYS is dominated by C-(A)-S-H nucleation and colloidal attractive interactions. Since peak 1 is higher than peak 2 in both mixtures, C-(A)-S-H nucleation plays a more critical role than colloidal attractive interactions at the testing age. Please also note that the SYS may be dictated mainly by colloidal interactions at a very early age and with a resting time of less than the percolation time of the mixture (about 5 min for mixtures PC and M75, see Fig. 9(d)). When the resting time is longer than the percolation time, the rigid interaction caused by C-(A)-S-H nucleation become more predominant, as reported by Roussel et al. [16].

4.3. Rigidification kinetics of static yield stress

In this study, a stronger particle interaction, induced by C-(A)-S-H nucleation and colloidal attractive forces, is observed for mixture M75 compared to mixture PC, as shown in Fig. 7(c). To determine the evolution of these particle interactions with time, the strain sweep tests were performed on mixtures PC, M75 and M75-SP1 using the same test protocol but with a longer resting time (60 min) and the test results are reported in Fig. 17. As can be observed, both peak 1 and peak 2 were significantly enhanced for mixtures PC and M75, with a substantial increase in peak 2 found for mixture M75-SP1. The increase in peak 1 appears to be attributed to the growth of C-(A)-S-H bonds between particles. Such bonds are only formed among Portland cement particles in mixture PC. In contrast, mixture M75 offers more possibilities for particle bonding, such as bonds between Portland cement and metakaolin (from calcined clay), Portland cement and limestone, and/or Portland cement and quartz (from calcined clay). However, no chemical bonds are formed between calcined clay, quartz, and limestone in the first 90 min of hydration.

According to Kumar et al. [52], fine limestone is a superior filler for promoting C-(A)-S-H growth compared to quartz. Similarly, Berodier and Scrivener [39] found that the use of fine limestone filler resulted in a shorter dormant period and higher acceleration of main hydration than quartz filler. The surface of limestone particles is fully covered by nuclei

even within 90 min of hydration, which was not observed in the case of quartz, slag, and fly ash. However, in this study, limestone powder with a coarser particle size than Portland cement did not show a strong enhancement in the strength of C-(A)-S-H bonds (see mixture L75, Fig. 7 (c)). Due to the large grain size, quartz (an impurity in calcined clay) is considered an inert filler, showing minor contribution to C-(A)-S-H nucleation as well. Therefore, in this context, we attribute the bond between metakaolin and Portland cement as the main cause of the increase in the strength of C-(A)-S-H bonds (peak 1). Ferron et al. [53] found that the minor addition of metakaolin (1.5 wt% of Portland cement) contributed to forming a more flocculated network than plain cement paste. Strong interparticle bonding that can resist significant breakage and erosion of flocs was observed. However, the authors [53] attributed this bonding to colloidal attractive interactions, instead of any chemical bridges.

The isothermal calorimetry results (Fig. 12 (e)) provide some evidence of chemical reaction promotion induced by metakaolin. It can be seen that the accumulated heat (in the period of 10–90 min) of mixture M75 was lower than that of mixture PC but higher than that of mixture L75. Both mixtures M75 and L75 generated more than 25 % of the cumulative heat of mixture PC. The additional heat in mixture M75 could be attributed to the enhanced cement hydration resulting from the filler effect and/or a potential reaction between the metakaolin and Portland cement. The increase in the dormant period (Fig. 12 (c)) may also reveal the consumption of CH by metakaolin at a very early age, as mentioned in Section 3.3. However, the mechanism of physicochemical bonding between Portland cement and metakaolin particles within the first 90 min of hydration remains an open question that requires further investigation. On the other hand, the higher SYS (CSR test) and peaks 1 and 2 (strain sweep test) of mixture M75, compared to mixture PC, could also be attributed to the enhanced particle interactions between Portland cement particles. As discussed earlier, the addition of calcined clay can reduce the WFT/particle distance, which may promote the flocculation and nucleation of cement particles, according to [14,39].

For mixture M75-SP1, peak 2 correlated to colloidal attractive force increased with an extension in resting time. To describe the colloidal attractive force between cement particles with SP, Gelardi and Flatt [36] introduced an interparticle force parameter $G_{(h)}$, considering the effect of van der Waals force $F_{(vdW)}$, electrostatic force $F_{(ES)}$, and steric repulsion force $F_{(SR)}$.

$$G_{(h)} = \frac{F_{(vdW)} - F_{(ES)} - F_{(SR)}}{\bar{a}} \quad (5)$$

where $\bar{a}$ represents the harmonic average radius, which can be regarded as a constant value in a cementitious material system. The increase in $G_{(h)}$ can be resulted from the increase of $F_{(vdW)}$ and/or the decrease of $F_{(ES)}$ and $F_{(SR)}$. As reported by Mantellato et al. [54], the amount of PCE polymers available for dispersing cementitious particles is reduced with precipitation of early-age hydration products. This is because the PCE polymers preferentially adsorb on the surface of hydrated aluminate phases and ettringite instead of cement particles. Owing to the reduction of dispersion force, the particle distance may be decreased, resulting in the growth of $F_{(vdW)}$. In addition, PCE polymers can also be adsorbed on the surface of calcined clay particles. Li et al. [55] revealed that the initially negatively charged surface of calcined clay can adsorb a large amount of Ca^{2+} from the pore solution, thereby enabling this process. The solid contacts (shear stress at large deformation) that may be related to the water absorption of agglomerated metakaolin particles were also enhanced after 60 min of resting time. However, the growth rate of colloidal attractive force and solid contacts is very limited after 50 min of material age, resulting in a slow evolution of SYS in mixture M75-SP1. The formation of C-(A)-S-H bridges is still hindered by the PCEs adsorbed on the surface of cement particles.

5. Conclusion

This study investigates the role of calcined clay in the static yield stress (SYS) evolution of fresh cementitious pastes with a high substitution rate (75 % by binder mass) of Portland cement with calcined clay and limestone. The visco-elasto-plastic behaviors, structural build-up, and early-age hydration kinetics of plain Portland cement (SVF: 43 %) and ternary-blended pastes (SVFs: 39 %, 43 %, and 55 %) during the first 90 min of hydration were quantified and compared. Results show that high calcined clay content not only alters particle packing but also strengthens particle interactions, accelerating SYS development.

At equivalent SVF, the ternary blend (M75) exhibited a lower SYS at 10 min but surpassed plain cement paste (PC) after 30 min. Initially, agglomerated fine metakaolin clusters retained free water, forming large capillary pores and lowering SYS. Over time, water absorption by these clusters reduced inter-particle distances, enhancing C-(A)-S-H nucleation and colloidal attractive forces, leading to a rapid rise in SYS. The "bonding" between metakaolin and cement particles likely contributed to this effect.

Increasing SVF using a PCE-based superplasticizer (SP) further reduced average inter-particle distance, increasing van der Waals forces. However, steric repulsion from SP initially suppressed colloidal attractions and hindered C-(A)-S-H bonding. Rigid grain-to-grain contacts were the primary reason for the highest initial SYS observed in the M75-SP1 mixture (0.8 % SP). At later stages, reduced SP effects allowed colloidal attractions to grow, but the lack of sufficient C-(A)-S-H nuclei slowed SYS evolution after 50 min.

These findings advance the understanding of limestone-calcined clay-based rheology, highlighting that calcined clay plays an active physicochemical role beyond acting as an inert filler. The study also suggests that optimized SP dosage can enhance SYS without severely sacrificing fluidity, benefiting 3D concrete printing applications. However, delayed SYS evolution due to weakened chemical bonding remains a challenge, especially for the rapid construction of slender printed structures.

CRediT authorship contribution statement

Yu Chen: Writing – review & editing, Writing – original draft, Visualization, Validation, Methodology, Investigation, Funding acquisition, Formal analysis, Data curation, Conceptualization. **Oğuzhan Çopuroğlu:** Writing – review & editing, Methodology, Conceptualization.

Declaration of Competing Interest

On behalf of all the authors, I declare that all authors have no conflict of interest regarding the content of the research as written in the submitted article.

Acknowledgments

Yu Chen would like to acknowledge the funding supported by National Natural Science Foundation of China (NSFC) (Grant No. 52402021), Natural Science Foundation of Jiangsu Province (Grant No. BK20241338), the Start-up Research Fund of Southeast University (Grant No. RF1028624009).

Appendix

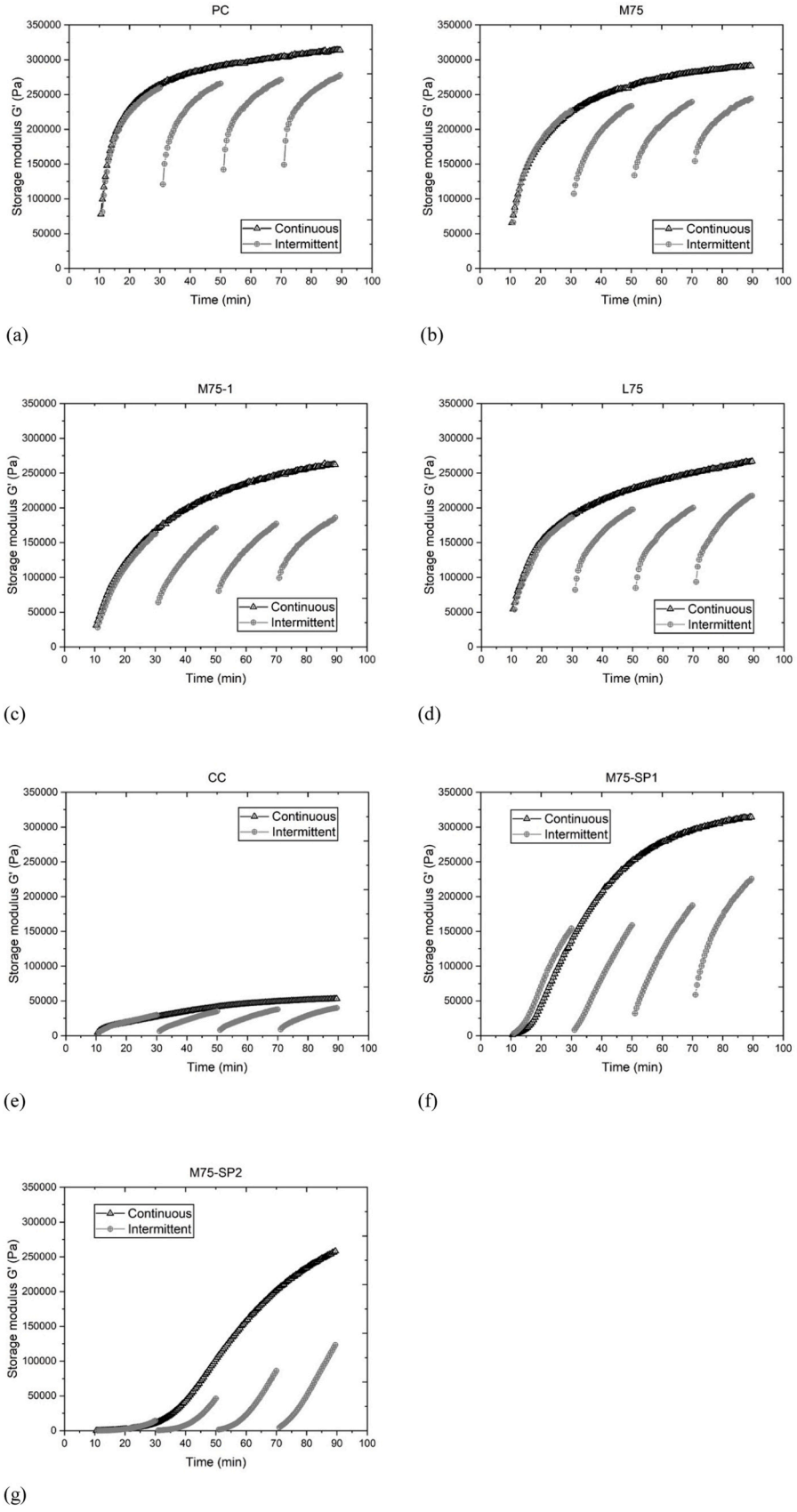

Fig. A1. Intermittent and continuous SAOS test results (G′ vs. material age): (a) Mixture PC; (b) Mixture M75; (c) Mixture M75–1; (d) Mixture L75; (e) Mixture CC; (f) Mixture M75-SP1; (g) Mixture M75-SP2

Data availability

Data will be made available on request.

References

[1] C. Shi, B. Qu, J.L. Provis, Recent progress in low-carbon binders, Cem. Concr. Res. 122 (2019) 227–250, https://doi.org/10.1016/j.cemconres.2019.05.009.

[2] M.C.G. Juenger, R. Snellings, S.A. Bernal, Supplementary cementitious materials: new sources, characterization, and performance insights, Cem. Concr. Res. 122 (2019) 257–273, https://doi.org/10.1016/j.cemconres.2019.05.008.

[3] B. Lothenbach, K. Scrivener, R.D. Hooton, Supplementary cementitious materials, Cem. Concr. Res. 41 (2011) 1244–1256, https://doi.org/10.1016/j.cemconres.2010.12.001.

[4] K. Scrivener, F. Martirena, S. Bishnoi, S. Maity, Calcined clay limestone cements (LC3), Cem. Concr. Res. 114 (2018) 49–56, https://doi.org/10.1016/j.cemconres.2017.08.017.

[5] R. Snellings, Assessing, understanding and unlocking supplementary cementitious materials, RILEM Tech. Lett. 1 (2016) 50, https://doi.org/10.21809/rilemtechlett.2016.12.

[6] M. Antoni, J. Rossen, F. Martirena, K. Scrivener, Cement substitution by a combination of metakaolin and limestone, Cem. Concr. Res. 42 (2012) 1579–1589, https://doi.org/10.1016/j.cemconres.2012.09.006.

[7] M. Sharma, S. Bishnoi, F. Martirena, K. Scrivener, Limestone calcined clay cement and concrete: a state-of-the-art review, Cem. Concr. Res. 149 (2021) 106564, https://doi.org/10.1016/j.cemconres.2021.106564.

[8] Y. Chen, S. He, Y. Zhang, Z. Wan, O. Çopuroğlu, E. Schlangen, 3D printing of calcined clay-limestone-based cementitious materials, Cem. Concr. Res. 149 (2021) 106553, https://doi.org/10.1016/j.cemconres.2021.106553.

[9] Y. Chen, S. He, Y. Gan, O. Çopuroğlu, F. Veer, E. Schlangen, A review of printing strategies, sustainable cementitious materials and characterization methods in the context of extrusion-based 3D concrete printing, J. Build. Eng. 45 (2022) 103599, https://doi.org/10.1016/j.jobe.2021.103599.

[10] N. Roussel, Rheological requirements for printable concretes, Cem. Concr. Res. 112 (2018) 76–85, https://doi.org/10.1016/j.cemconres.2018.04.005.

[11] T.R. Muzenda, P. Hou, S. Kawashima, T. Sui, X. Cheng, The role of limestone and calcined clay on the rheological properties of LC3, Cem. Concr. Compos. 107 (2020) 103516, https://doi.org/10.1016/j.cemconcomp.2020.103516.

[12] P. Hou, T.R. Muzenda, Q. Li, H. Chen, S. Kawashima, T. Sui, H. Yong, N. Xie, X. Cheng, Mechanisms dominating thixotropy in limestone calcined clay cement (LC3), Cem. Concr. Res. 140 (2021) 106316, https://doi.org/10.1016/j.cemconres.2020.106316.

[13] O. Canbek, Q. Xu, Y. Mei, N.R. Washburn, K.E. Kurtis, Predicting the rheology of limestone calcined clay cements (LC3): linking composition and hydration kinetics to yield stress through Machine Learning, Cem. Concr. Res. 160 (2022) 106925, https://doi.org/10.1016/j.cemconres.2022.106925.

[14] Y. Chen, Y. Zhang, S. He, M. Liang, Y. Zhang, E. Schlangen, Rheology control of limestone calcined clay cement pastes by modifying the content of fine- grained metakaolin, J. Sustain. Cem. Mater. 12 (2023) 1126–1140, https://doi.org/10.1080/21650373.2023.2169965.

[15] N. Roussel, H. Bessaies-Bey, S. Kawashima, D. Marchon, K. Vasilic, R. Wolfs, Recent advances on yield stress and elasticity of fresh cement-based materials, Cem. Concr. Res. 124 (2019) 105798, https://doi.org/10.1016/j.cemconres.2019.105798.

[16] N. Roussel, G. Ovarlez, S. Garrault, C. Brumaud, The origins of thixotropy of fresh cement pastes, Cem. Concr. Res. 42 (2012) 148–157, https://doi.org/10.1016/j.cemconres.2011.09.004.

[17] R. Sposito, M. Maier, N. Beuntner, K. Thienel, Physical and mineralogical properties of calcined common clays as SCM and their impact on flow resistance and demand for superplasticizer, Cem. Concr. Res. 154 (2022) 106743, https://doi.org/10.1016/j.cemconres.2022.106743.

[18] K. Scrivener, A. Ouzia, P. Juilland, A. Kunhi Mohamed, Advances in understanding cement hydration mechanisms, Cem. Concr. Res. 124 (2019) 105823, https://doi.org/10.1016/j.cemconres.2019.105823.

[19] F. Zunino, K. Scrivener, Insights on the role of alumina content and the filler effect on the sulfate requirement of PC and blended cements, Cem. Concr. Res. 160 (2022) 106929, https://doi.org/10.1016/j.cemconres.2022.106929.

[20] Y. Chen, Y. Zeng, M. Liang, S. He, O. Çopuroğlu, Blending Additional Calcium Hydroxide into LC3 with High Amount of Calcined Clay to Modify Fresh and Hardened Properties, Constr. Build. Mater. (Under Rev.). (n.d.).

[21] X. Dai, S. Aydın, M.Y. Yardımcı, K. Lesage, G. De Schutter, Effects of activator properties and GGBFS/FA ratio on the structural build-up and rheology of AAC, Cem. Concr. Res. 138 (2020) 106253, https://doi.org/10.1016/j.cemconres.2020.106253.

[22] A. Favier, G. Habert, J.B. D'Espinose De Lacaillerie, N. Roussel, Mechanical properties and compositional heterogeneities of fresh geopolymer pastes, Cem. Concr. Res. 48 (2013) 9–16, https://doi.org/10.1016/j.cemconres.2013.02.001.

[23] Q. Yuan, D. Zhou, K.H. Khayat, D. Feys, C. Shi, On the measurement of evolution of structural build-up of cement paste with time by static yield stress test vs. small amplitude oscillatory shear test, Cem. Concr. Res. 99 (2017) 183–189, https://doi.org/10.1016/j.cemconres.2017.05.014.

[24] M.A. Schultz, L.J. Struble, Use of oscillatory shear to study flow behavior of fresh cement paste, Cem. Concr. Res. 23 (1993) 273–282, https://doi.org/10.1016/0008-8846(93)90092-N.

[25] T.G. Mezger. The Rheology Handbook, 4th ed., Emerald Group Publishing Limited, 2009 https://doi.org/10.1108/prt.2009.12938eac.006.

[26] S. Ma, Y. Qian, S. Kawashima, Experimental and modeling study on the non-linear structural build-up of fresh cement pastes incorporating viscosity modifying admixtures, Cem. Concr. Res. 108 (2018) 1–9, https://doi.org/10.1016/j.cemconres.2018.02.022.

[27] X. Dai, S. Aydin, M.Y. Yardimci, G. De Schutter, Rheology and structural build-up of sodium silicate- and sodium hydroxide-activated GGBFS mixtures, Cem. Concr. Compos 131 (2022) 104570, https://doi.org/10.1016/j.cemconcomp.2022.104570.

[28] A. Favier, J. Hot, G. Habert, N. Roussel, J.B. D'Espinose De Lacaillerie, Flow properties of MK-based geopolymer pastes. A comparative study with standard Portland cement pastes, Soft Matter 10 (2014) 1134–1141, https://doi.org/10.1039/c3sm51889b.

[29] M.F. Alnahhal, T. Kim, A. Hajimohammadi, Distinctive rheological and temporal viscoelastic behaviour of alkali-activated fly ash/slag pastes: a comparative study with cement paste, Cem. Concr. Res. 144 (2021) 106441, https://doi.org/10.1016/j.cemconres.2021.106441.

[30] N. Roussel, A. Lemaître, R.J. Flatt, P. Coussot, Steady state flow of cement suspensions: a micromechanical state of the art, Cem. Concr. Res. 40 (2010) 77–84, https://doi.org/10.1016/j.cemconres.2009.08.026.

[31] V.N. Nerella, M.A.B. Beigh, S. Fataei, V. Mechtcherine, Strain-based approach for measuring structural build-up of cement pastes in the context of digital construction, Cem. Concr. Res. 115 (2019) 530–544, https://doi.org/10.1016/j.cemconres.2018.08.003.

[32] I. Ivanova, V. Mechtcherine, Possibilities and challenges of constant shear rate test for evaluation of structural build-up rate of cementitious materials, Cem. Concr. Res. 130 (2020) 105974, https://doi.org/10.1016/j.cemconres.2020.105974.

[33] D. Marchon, S. Kawashima, H. Bessaies-Bey, S. Mantellato, S. Ng, Hydration and rheology control of concrete for digital fabrication: potential admixtures and cement chemistry, Cem. Concr. Res. 112 (2018) 96–110, https://doi.org/10.1016/j.cemconres.2018.05.014.

[34] D. Marchon, R.J. Flatt. Impact of Chemical Admixtures on Cement Hydration, Elsevier Ltd, 2015, 10.1016/B978-0-08-100693-1.00012-6.

[35] N. Roussel, H. Bessaies-Bey, S. Kawashima, D. Marchon, K. Vasilic, R. Wolfs, Recent advances on yield stress and elasticity of fresh cement-based materials, Cem. Concr. Res. 124 (2019) 105798, https://doi.org/10.1016/j.cemconres.2019.105798.

[36] G. Gelardi, R.J. Flatt. Working Mechanisms of Water Reducers and Superplasticizers, Elsevier Ltd, 2015, 10.1016/B978-0-08-100693-1.00011-4.

[37] A.M. Mostafa, A. Yahia, New approach to assess build-up of cement-based suspensions, Cem. Concr. Res. 85 (2016) 174–182, https://doi.org/10.1016/j.cemconres.2016.03.005.

[38] A.M. Mostafa, A. Yahia, Physico-chemical kinetics of structural build-up of neat cement-based suspensions, Cem. Concr. Res. 97 (2017) 11–27, https://doi.org/10.1016/j.cemconres.2017.03.003.

[39] E. Berodier, K. Scrivener, Understanding the filler effect on the nucleation and growth of C-S-H, J. Am. Ceram. Soc. 97 (2014) 3764–3773, https://doi.org/10.1111/jace.13177.

[40] F. Zunino, K. Scrivener, The influence of the filler effect on the sulfate requirement of blended cements, Cem. Concr. Res. 126 (2019) 105918, https://doi.org/10.1016/j.cemconres.2019.105918.

[41] J. Lapeyre, A. Kumar, Influence of pozzolanic additives on hydration mechanisms of tricalcium silicate, J. Am. Ceram. Soc. 101 (2018) 3557–3574, https://doi.org/10.1111/jace.15518.

[42] Y. Qian, S. Kawashima, Distinguishing dynamic and static yield stress of fresh cement mortars through thixotropy, Cem. Concr. Compos 86 (2018) 288–296, https://doi.org/10.1016/j.cemconcomp.2017.11.019.

[43] K. Vance, A. Kumar, G. Sant, N. Neithalath, The rheological properties of ternary binders containing Portland cement, limestone, and metakaolin or fly ash, Cem. Concr. Res. 52 (2013) 196–207, https://doi.org/10.1016/j.cemconres.2013.07.007.

[44] W.W.S. Fung, A.K.H. Kwan, Role of water film thickness in rheology of CSF mortar, Cem. Concr. Compos 32 (2010) 255–264, https://doi.org/10.1016/j.cemconcomp.2010.01.005.

[45] H. Liu, X. Sun, H. Du, H. Lu, Y. Ma, W. Shen, Z. Tian, Effects and threshold of water film thickness on multi-mineral cement paste, Cem. Concr. Compos 112 (2020) 103677, https://doi.org/10.1016/j.cemconcomp.2020.103677.

[46] J.J. Chen, A.K.H. Kwan, Superfine cement for improving packing density, rheology and strength of cement paste, Cem. Concr. Compos 34 (2012) 1–10, https://doi.org/10.1016/j.cemconcomp.2011.09.006.

[47] L.G. Li, X.Q. Chen, S.H. Chu, Y. Ouyang, A.K.H. Kwan, Seawater cement paste: effects of seawater and roles of water film thickness and superplasticizer dosage, Constr. Build. Mater. 229 (2019) 116862, https://doi.org/10.1016/j.conbuildmat.2019.116862.

[48] P. Coussot. Introduction to the Rheology of Complex Fluids, Woodhead Publishing, 2011, 10.1016/B978-0-85709-028-7.50001-7.

[49] A. Perrot, T. Lecompte, H. Khelifi, C. Brumaud, J. Hot, N. Roussel, Yield stress and bleeding of fresh cement pastes, Cem. Concr. Res. 42 (2012) 937–944, https://doi.org/10.1016/j.cemconres.2012.03.015.

[50] R.J. Flatt, Dispersion forces in cement suspensions, Cem. Concr. Res. 34 (2004) 399–408, https://doi.org/10.1016/j.cemconres.2003.08.019.

[51] V.N. Nerella, M.A.B. Beigh, S. Fataei, V. Mechtcherine, Strain-based approach for measuring structural build-up of cement pastes in the context of digital construction, Cem. Concr. Res. 115 (2019) 530–544, https://doi.org/10.1016/j.cemconres.2018.08.003.

[52] A. Kumar, T. Oey, G. Falzone, J. Huang, M. Bauchy, M. Balonis, N. Neithalath, J. Bullard, G. Sant, The filler effect: the influence of filler content and type on the hydration rate of tricalcium silicate, J. Am. Ceram. Soc. 100 (2017) 3316–3328, https://doi.org/10.1111/jace.14859.
[53] R.D. Ferron, S. Shah, E. Fuente, C. Negro, Aggregation and breakage kinetics of fresh cement paste, Cem. Concr. Res. 50 (2013) 1–10, https://doi.org/10.1016/j.cemconres.2013.03.002.
[54] S. Mantellato, M. Palacios, R.J. Flatt, Relating early hydration, specific surface and flow loss of cement pastes, Mater. Struct. Constr. 52 (2019) 1–17, https://doi.org/10.1617/s11527-018-1304-y.
[55] R. Li, L. Lei, T. Sui, J. Plank, Effectiveness of PCE superplasticizers in calcined clay blended cements, Cem. Concr. Res. 141 (2021) 106334, https://doi.org/10.1016/j.cemconres.2020.106334.